Simulation on buildup of electron cloud in a proton circular accelerator*

LI Kai-Wei(李开玮)[1,2] LIU Yu-Dong(刘瑜冬)[1;1)]

[1] Dongguan Campus, Institute of High Energy Physics, Chinese Academy of Sciences, Dongguan 523803, China
[2] University of Chinese Academy of Sciences, Beijing 100049, China

Abstract: Electron cloud interaction with high energy positive beams are believed responsible for various undesirable effects such as vacuum degradation, collective beam instability and even beam loss in high power proton circular accelerators. An important uncertainty in predicting electron cloud instability lies in the detailed processes of the generation and accumulation of the electron cloud. The simulation on the build-up of electron cloud is necessary to further studies on beam instability caused by electron clouds. The China Spallation Neutron Source (CSNS) is an intense proton accelerator facility now being built, whose accelerator complex includes two main parts: an H-linac and a rapid cycling synchrotron (RCS). The RCS accumulates the 80 MeV proton beam and accelerates it to 1.6 GeV with a repetition rate of 25 Hz. During beam injection with lower energy, the emerging electron cloud may cause serious instability and beam loss on the vacuum pipe. A simulation code has been developed to simulate the build-up, distribution and density of electron cloud in CSNS/RCS.

Key words: electron cloud, instability, electron multipacting, beam loss

PACS: 29.27.Bd **DOI:** 10.1088/1674-1137/39/10/107002

1 Introduction

In high intensity proton circular accelerators, the electron cloud effect is considered to be one of the main sources of beam instability, which can lead to uncontrolled beam loss [1]. This electron proton instability has been observed and confirmed in many commissioned proton circular accelerators, such as LANL PSR [2], KEK Booster [3], CERN PS [4] and SNS in ORNL [5]. During proton beam operation, the main primary electrons produced by proton losses at the chamber surface are attracted and accelerated by the body part of the bunch, then released at the bunch tail or bunch spacing. The secondary electrons are produced and amplified when these accelerated electrons hit the chamber wall. This secondary electron multipacting is the main source of the electron cloud.

A high intensity proton accelerator facility to act as a neutron source has been proposed in the past ten years and is being built in China, named the China Spallation Neutron Source (CSNS) [6]. The facility is equipped with an H-linac and a rapid cycling synchrotron (RCS). The RCS is designed to accumulate a proton beam and accelerate it from 80 MeV to 1.6 GeV. The accumulated particles in the RCS can reach to 7.8×10^{12} protons in a bunch with length about several tens of meters. Such high population and long bunches circulating in the RCS may lead to a denser electron cloud. A simulation code has been developed and benchmarked to ascertain the detailed establishment of an electron cloud in the CSNS/RCS. The physical mechanism of primary electron production, its dynamics, secondary electron emission and electron accumulation is described in Section 2 of this paper. By tracking dynamics of electrons with the physical model in Section 2, a simulation code for obtaining the distribution and density of the electron cloud in proton-circulated accelerators has been developed and benchmarked with other machines. With the beam parameters of RCS/CSNS, the process of electron cloud buildup is studied in different simulation conditions such as average beam loss factor, secondary electron yields, transverse and longitudinal beam profile, and beam intensity. Most of the simulations are performed mainly in a field-free region, and the contribution of the dipole magnetic field is also investigated. The comprehensive simulation of an electron cloud in RCS/CSNS gives a quantitative relation between electron density and beam parameters, which is meaningful to the construction of RCS/CSNS (Table 1).

2 Physical model

The electron sources in a proton circular accelerator may be classified into (1) electrons stripped at the injec-

Received 9 December 2014, Revised 13 March 2015

∗ Supported by National Natural Science Foundation of China (11275221, 11175193)

1) E-mail: liuyd@ihep.ac.cn. Corresponding author

tion region; (2) electrons produced by proton losses incident on the vacuum chamber at grazing angles; (3) secondary electron emission process; and (4) electrons produced by residual gas ionization. The stripped electrons generated near the stripping foil can be absorbed by installing a special electron collector at the injection region [7]. The yield of ionization electrons is determined by the ionization cross section and the vacuum pressure in the beam chamber. Because of the lower vacuum pressure about 10^{-7} Pa and ionization cross section for CO and H_2 of approximately 1.3 MBar and 0.3 MBar respectively, the ionization electrons can be ignored in the simulation. In the electron dynamic tracking for RCS/CSNS, the primary electrons produced by proton losses and secondary electrons are considered.

Table 1. The main parameters of the RCS/CSNS.

parameters	injection phase	extraction phase
circumference C/m	227.92	227.92
energy E/GeV	0.08	1.6
bunch population $N_{\rm p}$ (10^{13})	1.56	1.56
revolution frequency ω/MHz	3.20	6.78
bunch length $\sigma_{\rm p}$/m	48.93	22.285
harmonic number h	2	2
beam transverse size σ_x, σ_y/cm	1.5, 1.5	1.2, 1.2
pipe radius b/cm	10	10

When primary electrons are emitted from the pipe wall, they have interaction with the proton beam and move towards the opposite wall, then hit the wall after a period of transit. These striking electrons may produce secondary electrons if their energy is high enough. The fraction between the emission electrons from the pipe surface and the total incident electrons is defined as secondary electron yield (SEY). If SEY is above 1, electron multipacting will happen. Actually, the secondary electrons include two types: the elastic backscattered electrons and true secondary electrons. The yields of the true secondary electrons and elastic backscattered electrons can be expressed with formula (1) and (2) [8], respectively. In the formula, $\delta_{\max}$ is the maximum secondary emission yield for perpendicular incidence, and $\varepsilon_{\max}$ presents the incidence electron energy with maximum secondary emission yield $\delta_{\max}$. Here, $E_{\rm p}$ is the energy of the electron, θ the angle of the incidence electrons and $\hat{\delta}_{\rm e}$, $\delta_{\rm e,\infty}$, Δ and $E_{\rm e}$ are the experimental fitting parameters decided by the pipe material, with $\hat{\delta}_{\rm e}$=0.1, $\delta_{\rm e,\infty}$=0.02 and Δ=$E_{\rm e}$=5 eV [8].

$$\delta_{\rm se}(E_{\rm p},\theta)=\delta_{\max}\times\frac{1.44\times(E_{\rm p}/\varepsilon_{\max})}{0.44+(E_{\rm p}/\varepsilon_{\max})^{1.44}}\exp(0.5\times(1-\cos\theta)). \quad (1)$$

$$\delta_{\rm e}(E_{\rm p})=\delta_{\rm e,\infty}+\hat{\delta}_{\rm e}-\delta_{\rm e,\infty}\exp\left(\frac{-(E_{\rm p}-E_{\rm e})^2}{2\Delta^2}\right). \quad (2)$$

The results on SEY with and without elastic backscattered electrons are illustrated in Fig. 1. It is clear that the elastic portion has more influence in the lower energy region. In the simulation, these two types of secondary electrons are included.

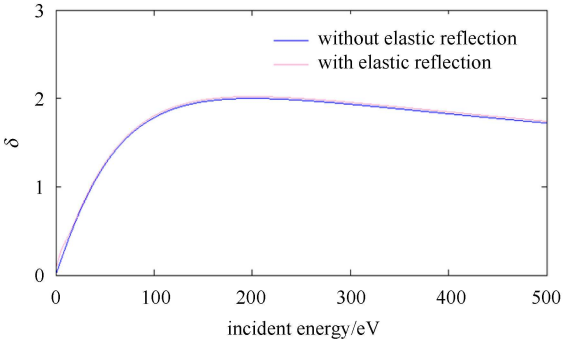

Fig. 1. (color online) Secondary electron yield in different incident electron energy.

In the magnetic-field-free region, the electrons move under the space-charge fields of the proton beam and between other electrons. For long proton bunches, the longitudinal space-charge field can be ignored due to slow potential variations in the longitudinal direction and the symmetry of the longitudinal beam profile, that traps the particles longitudinally. Therefore, the electrons mainly move under the beam transverse fields. For a cylindrical beam with uniform and Gaussian transverse distribution, the space-charge fields are expressed respectively as

$$E_r(t)=\begin{cases}\dfrac{\lambda(t)}{4\pi\varepsilon_0}\dfrac{2}{r}\,(r>\sigma_r),\\[2ex] \dfrac{\lambda(t)}{4\pi\varepsilon_0}\dfrac{2r}{\sigma_r^2}\,(r<\sigma_r),\end{cases} \quad (3)$$

$$E_r(t)=\frac{\lambda(t)}{4\pi\varepsilon_0}\left[1-\exp\left(-\frac{r^2}{2\sigma_r^2}\right)\right]\frac{2}{r}, \quad (4)$$

where $\lambda(t)$ is the beam line density, ε_0 is the permittivity of vacuum, and σ_r is the beam transverse size. In fact, the space-charge fields of any spatial particle distribution can be obtained by numerical evaluation with the particle in cell (PIC) method, which meshes the particles in a three dimensional grid and makes two-dimensional fast Fourier transforms (FFT) in the transverse grids for each longitudinal slice to compute the potential on every grid point [9]. The electric field comparison between numerical solution and analytical solution to uniform and Gaussian distributed charge are shown in Fig. 2. It is clear the numerical solution fits well to the analytical results.

During the passage of the proton bunch, the electrons experience the beam action and make a nearly periodic oscillation with a slow time-dependence given by the beam line density $\lambda(t)$. Assuming the bunch is uniform in the longitudinal direction with bunch population

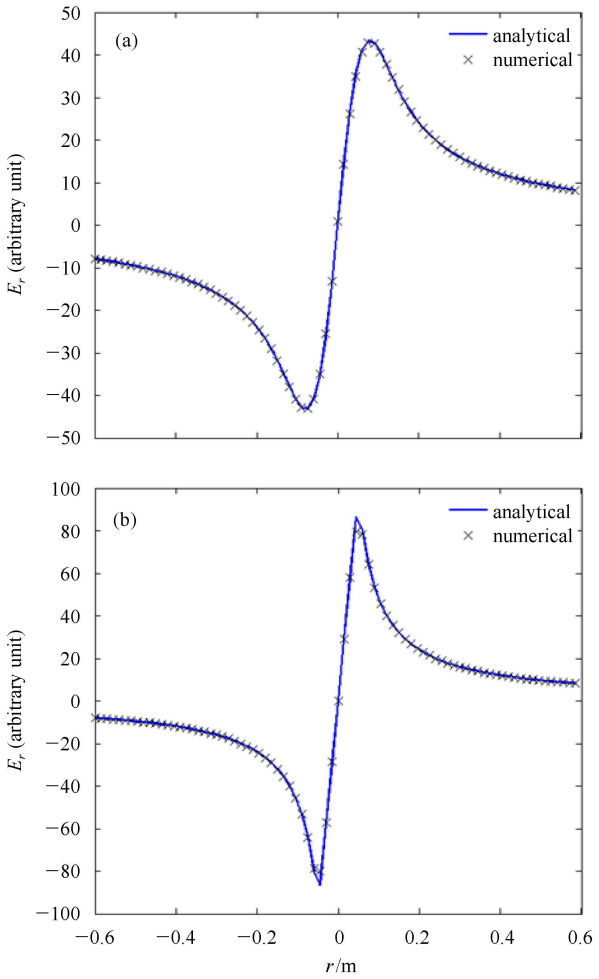

Fig. 2. (color online) Electric field with different particle distributions ((a): Gaussian; (b): uniform).

1.56×10^{13} in CSNS/RCS, the oscillation frequency of the electron ranges from 20.23 MHz to 134.84 MHz.

In the simulation model, electron cloud formation is estimated by tracking the motion of electrons produced by the primary and the secondary electron emissions. The vacuum chamber is assumed to be a cylindrical perfectly conducting pipe. The primary electrons generated by lost protons hitting the vacuum chamber wall is $Y\cdot P_{\rm loss}$ per turn for the whole ring, where Y is the effective electron yield per lost proton, and $P_{\rm loss}$ is the proton loss rate per turn for the whole ring per beam proton. The lost-proton time distribution is proportional to the instantaneous bunch intensity. The electrons are then represented by macroparticles. The secondary electron mechanism adds to these a variable number of macroparticles, generated according to the SEY model mentioned above. The proton bunch is sliced along the longitudinal direction into equal-size steps and each slice has a local proton density $\lambda(t_{\rm i})$. Electrons are tracked step-by-step along the passage of the proton beam. The equation of motion for electrons is expressed by

$$\frac{{\rm d}^2x(t)}{{\rm d}t^2}=-2\lambda_{\rm p}(t_{\rm i})r_{\rm e}c^2F_{\rm G}[x(t)], \tag{5}$$

where $r_{\rm e}$ is the classical electron radius, and $F_{\rm G}$ is the normalized electric force determined by Eqs. (3) and (4). For proton bunches in CSNS/RCS, the longitudinal profile is a sinusoidal function expressed as

$$\lambda_{\rm p}(t_{\rm i})=\frac{\pi N_{\rm p}}{2\sigma_{\rm p}}\sin\left(\frac{\pi v t_{\rm i}}{\sigma_{\rm p}}\right), \tag{6}$$

where $\sigma_{\rm p}$ is the longitudinal length of the proton bunch and v is the bunch velocity.

3 Simulation results

Based on the physical model described in Section 2, a simulation code was developed independently to understand the buildup of electron cloud in proton circular accelerators. After verifying the validity of the simulation by benchmarking electron cloud density in J-PARC,

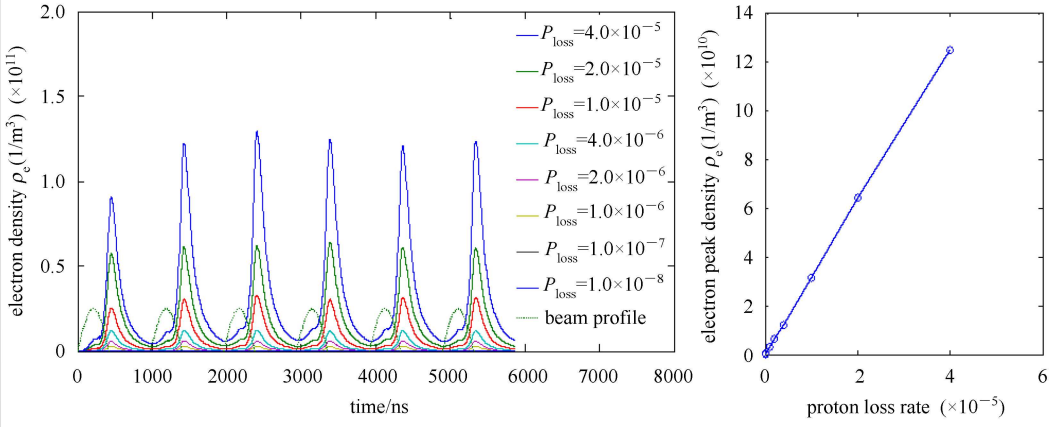

Fig. 3. (color online) The densities of electron cloud with different proton loss rates.

LANL PSR and ORNL SNS, the buildup of the electron cloud in CSNS/RCS is simulated with different parameters, such as proton loss rate, SEY, beam intensity and bunch transverse size. For a high intensity proton accelerator, the common requirement of loss power for maintenance is lower than 1 W/m. Assuming the beam loss happens in the first several hundred turns and every lost proton can produce 100 electrons [10], the densities of electron cloud for a series of $P_{\rm loss}$ are shown in Fig. 3.

It is clear that the peak density of the electron cloud is linear with the proton loss rate because of the thinner density of the electron cloud, whose line density $\lambda_{\rm e}$ is only about 2% the proton average line density $\lambda_{\rm p}$. The transverse distribution of electrons during the passage of the bunch CSNS/RCS 80 MeV at injection is shown in Fig. 4.

It is clear the electrons are produced near the pipe wall and distributed widely at the start of the interaction with the bunch. Then these electrons are gathered to the beam vicinity and the cloud size is comparable to the beam size. After the bunch passage and without interaction, these accumulated electrons splash in the vacuum pipe. The last picture shows the electron distribution before the next bunch comes, with a considerable quantity of electrons remaining in the chamber. This quantity depends on the ring and beam parameters. During the passage of the next bunch, the same process will happen again.

The secondary electrons produced by primary electron incidence on the pipe wall will be the main portion of the electron cloud when the SEY is above 1.0. The TiN

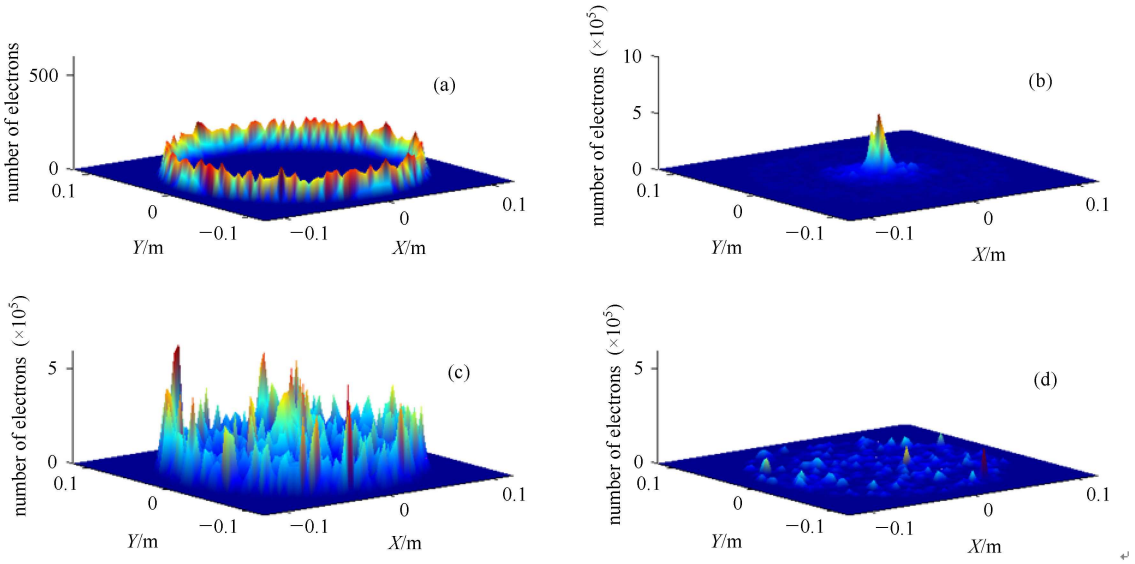

Fig. 4. (color online) Transverse distribution of electron cloud during a bunch passage (a: bunch head; b: bunch center; c: bunch tail; d: bunch gap).

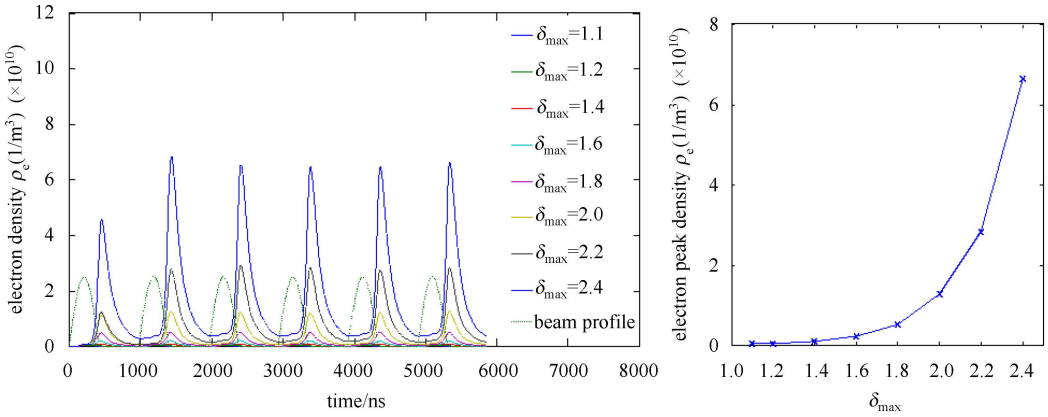

Fig. 5. (color online) The electron cloud with various $\delta_{\rm max}$.

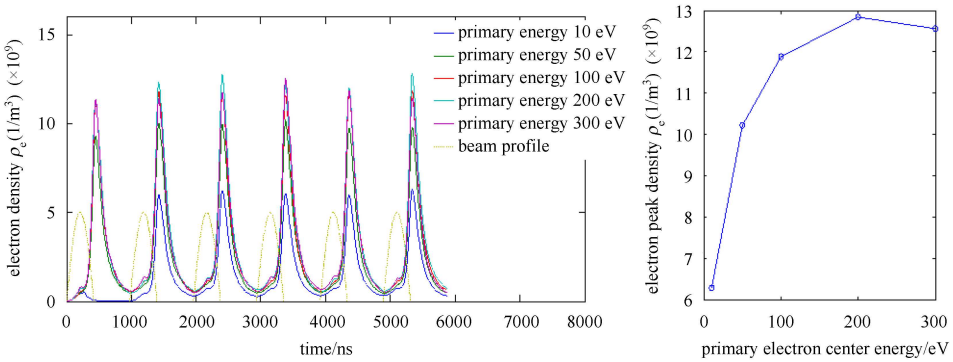

Fig. 6. (color online) The electron cloud vs various primary electron energy.

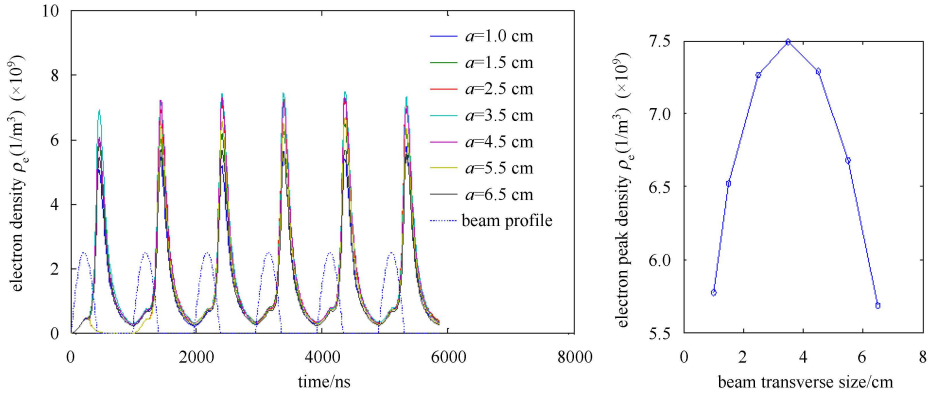

Fig. 7. (color online) Electron cloud density vs beam transverse size.

coating inside the vacuum pipe can suppress the maximum secondary electron yield to 1.3. The electron cloud amplification in various $\delta_{\max}$ is simulated for CSNS/RCS and the results are shown in Fig. 5. It is clear that the peak electron cloud density is sensitive to the maximum secondary electron yield. So the most efficient method to cure the electron cloud is surface treatment to reduce $\delta_{\max}$ below 1.3.

The energy of primary electrons is decided by the loss protons. In order to understand the relation between primary electron characteristics and electron cloud, the development of electron cloud for different primary electron energies is simulated and shown in Fig. 6. The secondary electron yield parameters, $\delta_{\max}$=2.0 and $\varepsilon_{\max}$=200 eV are adopted in the calculation. The electron cloud density in Fig. 6 varies as the SEY curve because of the electron multipacting dependence on the incident energy.

The beam transverse size also has much influence on the saturation density of the electron cloud because of the beam space-charge fields expressed in Eqs. (3) and (4). The simulation of electron cloud under different beam transverse size is shown in Fig. 7. Initially, the narrow beam transverse size leads to a stronger electronic field and the electron energy gain exceeds the SEY parameter $\varepsilon_{\max}$. With the beam size extension, the electron energy gain decreases to $\varepsilon_{\max}$ and the electron multipacting is serious enough to cause the highest cloud density. Broadening the beam size gradually, electron energy gain drops lower to $\varepsilon_{\max}$ and the cloud density decreases correspondingly.

The electron cloud buildup with different beam intensity is plotted in Fig. 8. With the stronger beam intensity, the primary electrons produced by the beam loss increase correspondingly and their energy gain is enhanced simultaneously. These reasons lead to the electron cloud density rising exponentially, shown in Fig. 8. When the beam intensity reaches 4.0×10^{13}/bunch, the peak density of electrons cloud is more than 7.6×10^{11}/m^3.

We now discuss the electron cloud buildup in magnetic field. The beam chamber is covered with various magnets including bending, quadrupole, and higher order magnets in the actual rings. The field-free regions and bending magnets occupy the biggest part of the rings. In bending magnets with a strong dipole field, electrons undergo cyclotron motion with a small radius (<1 mm) and at a high frequency (>10 GHz). The electron cloud buildup in a dipole magnet is plotted in Fig. 9. Because of the cyclotron motion caused by the dipole

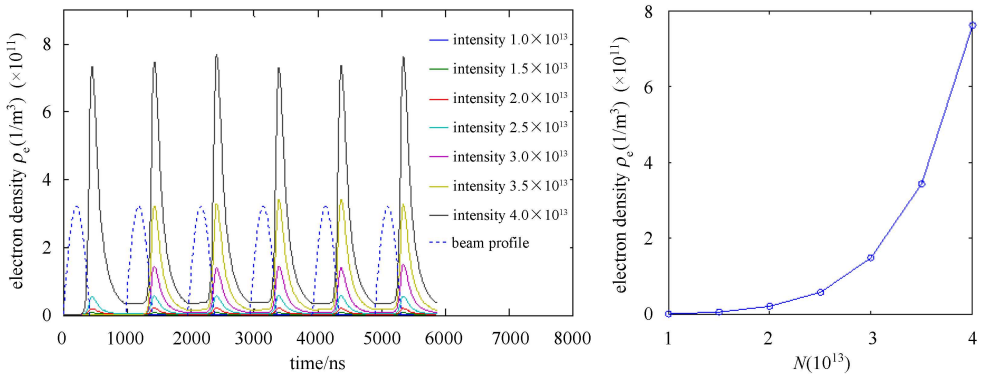

Fig. 8. (color online) Electron cloud density vs different beam intensity.

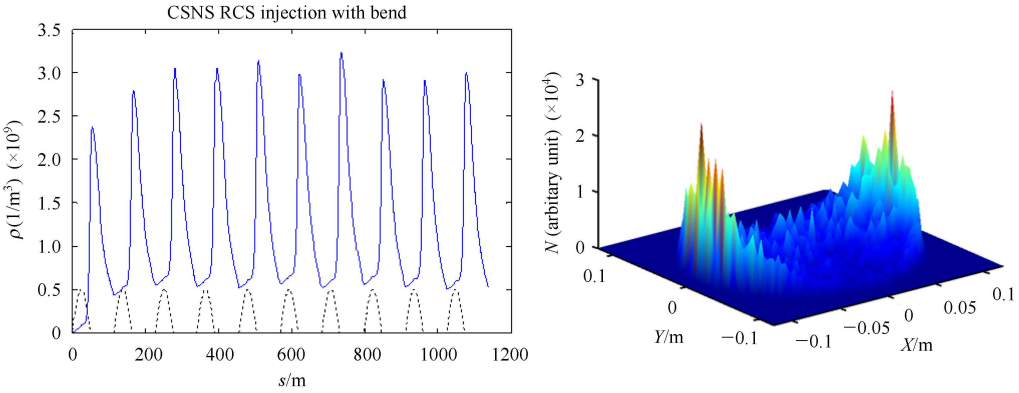

Fig. 9. (color online) Electron cloud in dipole magnets.

field, a considerable fraction of the electrons cannot approach the beam, therefore they do not get sufficient energy for the multipacting. So the dipole fields have the effect of suppressing the buildup of an electron cloud.

4 Conclusion

In the instance of CSNS/RCS, the buildup of the electron cloud in a circular proton accelerator was investigated. A computer simulation code was developed to study the accumulation process of an electron cloud. In the simulation model primary electrons appear due to proton loss on the wall of the vacuum pipe and the secondary electron emission model is also included. The calculation proved the application on TiN coating to reduce the secondary yield is a very powerful cure for the electron cloud. An investigation on the electron cloud buildup with various beam parameters such as beam intensity, transverse size and proton loss rate, was done in detail. The formation of the electron cloud in dipole field was also simulated to testify the suppression of electron multipacting. All these simulations will be meaningful to understand the interaction between electrons and high intensity proton beam in circular accelerators.

References

1 Neuffer D, Colton E et al. Nucl. Instrum. Methods A, 1992, **321**: 1–12
2 Macek R et al. Overview of the Program Plan and the Experimental Results from PSR. In: LBLN Workshop on the e-p instability, November, 2000. 20
3 Irie Y et al. In: KEK Proceedings 97-17, 1997. 247
4 Cappi R, Metral G. http://www.cern.ch/PSdoc/ppc/md/md980716/epinstab.html
5 Danilov V V et al. Accumulation of High Intensity Beam and First Observations of Instabilities in the SNS Accumulator Ring. In: HB2006, 2006. 59
6 WANG S, FANG S X, FU S N et al. Chin. Phys. C, 2009, **33**: 1–3
7 WANG L F, Raparia D, WEI J, ZHANG S Y. Physical Review Special Topics - Accelerators and Beams, 2004, **7**: 034401
8 Furman M A, Lambertson G R. The Electron Cloud Effect in the arcs of the PEP-Ⅱ Positron Ring. In: KEK Proceedings 97-17, 1997. 170
9 JI Qiang et al. Physical Review Special Topics - Accelerators and Beams, 2002, **5**: 104402
10 Thieberger P et al. Phys. Rev. A, 2000, **61**: 042901